

Explaining the ANITA Anomaly with Inelastic Boosted Dark Matter

Lucien Heurtier,^{1,*} Doojin Kim,^{1,†} Jong-Chul Park,^{2,‡} and Seodong Shin^{3,§}

¹*Department of Physics, University of Arizona, Tucson, AZ 85721, USA*

²*Department of Physics, Chungnam National University, Daejeon 34134, Republic of Korea*

³*Department of Physics & IPAP, Yonsei University, Seoul 03722, Republic of Korea*

We propose a new physics scenario in which the decay of a very heavy dark-matter candidate which does not interact with the neutrino sector could explain the two anomalous events recently reported by ANITA. The model is composed of two components of dark matter, an unstable dark-sector state, and a massive dark gauge boson. We assume that the heavier dark-matter particle of EeV-range mass is distributed over the galactic halo and disintegrates into a pair of lighter – highly boosted – dark-matter states in the present universe which reach and penetrate the Earth. The latter scatters *inelastically* off a nucleon and produces a heavier dark-sector unstable state which subsequently decays back to the lighter dark matter along with hadrons, which induce Extensive Air Showers, via on-/off-shell dark gauge boson. Depending on the mass hierarchy within the dark sector, either the dark gauge boson or the unstable dark-sector particle can be long-lived, hence transmitted significantly through the Earth. We study the angular distribution of the signal and show that our model favors emergence angles in the range $\sim 25^\circ - 35^\circ$ if the associated parameter choices bear the situation where the mean free path of the boosted incident particle is much larger than the Earth diameter while its long-lived decay product has a decay length of dimensions comparable to the Earth radius. Our model, in particular, avoids any constraints from complementary neutrino searches such as IceCube or the Auger observatory.

I. INTRODUCTION

The ANtarctic Impulsive Transient Antenna (ANITA) Collaboration recently reported two anomalous upward-moving cosmic-ray-like events whose inferred energy lies in $\sim 0.5 - 1$ EeV [1, 2]. Within the framework of the Standard Model (SM), one could envision, for example, an EeV-scale tau-neutrino traversing the Earth and converting to a tau lepton which is responsible for producing an Extensive Air Showers (EAS) in the atmosphere after escaping the surface of the Earth. However, given the typical amount of energy that such a neutrino would have to carry, and the interaction strength of the latter with nuclei, its propagation through the Earth on large distances is extremely unlikely to let a subsequent tau lepton escape the Earth at a sizable emergence angle (see also FIG. 8 for notational conventions). Indeed, a boosted tau neutrino having an energy of $\mathcal{O}(1)$ EeV has a transmission probability lower than 10^{-6} to induce an EeV-scale tau lepton even if one includes multiple $\tau - \nu_\tau$ regenerations [2], and a dedicated study in Ref. [3] has concluded that SM explanations are excluded by (at least) 5σ confidence. Furthermore, Ref. [4] explored the hypothesis of a tau-neutrino origin together with a dedicated acceptance estimate, and reached the conclusion that the ANITA events disfavor a diffuse tau-neutrino interpretation in comparison with the Auger [5] and IceCube [6] upper limits. This suggests that new physics should come into play in order to accommodate the anomaly in a self-

consistent manner, stimulating the theory community to propose various beyond-the-SM (BSM) scenarios.

For completeness, we should mention that the ANITA anomalous events might be explained in pure SM interpretations which were recently proposed. A downward-moving high-energy cosmic rays might indeed be able to produce the ANITA's inverted polarity signals through coherent transition radiation from the geomagnetic-induced current in the associated air showers [7] or could be reflected by sub-layer of the ice-sheet of the Antarctic [8]. Such proposals remain for now speculative and still require experimental confirmations, in particular from the ANITA Collaboration itself, and therefore we shall focus in this work on the possibility that such events are a sign of new physics.

Among other attempts, several trials assumed the existence of non-SM neutrino species in order to address the signal. For example, the authors of Ref. [9, 10] adopt sterile neutrinos induced by Ultra High Energy (UHE) cosmic rays as “agents” propagating through the Earth in order to explain the ANITA events, while Ref. [11] interprets the signal with lepto-quark-mediated sterile neutrinos. By contrast, Ref. [12] hypothesizes super-heavy right-handed neutrinos captured in the Earth which subsequently decay to active neutrinos in the vicinity of the Earth surface. Some of the latest attempts imagine new physics scenarios within the supersymmetric framework. Examples include interpretations utilizing next-to-lightest supersymmetric tau lepton (i.e., “stau”) [3], long-lived bino in R-parity violating supersymmetry [13], and neutrino-initiated supersymmetric sphaleron transitions [14]. In contrast to the approaches taken in preceding works, the authors of Refs. [15] and [16] explored the possibility that the flux of boosted particles necessary to explain the signal is due to the decay of a super-

* heurtier@email.arizona.edu

† doojinkim@email.arizona.edu

‡ jcpark@cnu.ac.kr

§ seodongshin@yonsei.ac.kr

heavy dark-matter particle in the Milky Way. In [15] the ANITA anomalous events are explained with a dark-matter species decaying into a pair of right-handed neutrinos, which later on convert into taus inside the Earth and produce high-energy EAS in the atmosphere. In a complementary manner, also using the decay of a super-heavy dark-matter particle, the authors of Ref. [16] proposed an interpretation in terms of the Askaryan emission created by elastic scattering of feebly interacting particles within the ice sheet. The authors of Ref. [17] finally reviewed different topologies of processes which could explain the signal with EAS and proposed a model in which a heavy dark-matter decays into a boosted light component which converts into taus after scattering within the Earth. As another recent BSM interpretation, the authors of Ref. [18] argued that the reflection of radio pulses could reproduce the ANITA signals via axion-photon conversion.

As a generic feature of most of the aforementioned interpretations, we point out that previous works rely on the interaction which might exist between new-physics states and ordinary SM neutrinos in order to induce the relevant experimental signatures. The new states thus *effectively* “transport” the neutrinos through the Earth to enhance the chance that they convert into leptons in the vicinity of the surface.

While producing leptons inside the Earth from the conversion of neutrinos is probably the most natural *SM-friendly* interpretation at low energy, the situation is radically different at very high energy since the neutrino is not a good candidate to help propagating through the Earth on large distances. Moreover, there are no compelling reasons that neutrinos are necessary ingredients to explain the ANITA anomaly. Indeed, the only requirement for ANITA to detect a signal is that a significant electric field is locally produced around the detector. Therefore, as far as EAS are concerned, the production of any boosted hadronic final states in the atmosphere, whatever its parent particle is, would suffice to propose an interpretation for the anomalous events reported by the Collaboration.

Furthermore, the connection between the neutrino sector and new-physics states has been thoroughly probed by different experiments in the past and eventually leads to tensions between existing experimental constraints and the parameter choices required in order to fit the data. In particular, the production of highly boosted – and therefore very long-lived – τ leptons close to the Earth surface, which can pass through terrestrial detectors such as IceCube before decaying in the atmosphere, may leave sizable signatures which should already have been observed.

In light of these considerations, we propose a dark-matter scenario not accompanying the production of SM leptons inside the Earth (in contrast to that in [15] and [16]) in order to explain the two ANITA anomalous events. The model that we consider is built upon a non-minimal dark sector scenario, containing

- ϕ , a super-heavy scalar dark matter,
- χ_1 , a light fermionic dark-matter component,
- χ_2 , an unstable fermionic dark-sector state, and
- X , a dark gauge boson interacting with the aforementioned fermionic states and mixing with the SM photon through kinetic mixing.

We assume that the whole signal process sketched in FIG. 1 begins with the decay of ϕ into a pair of χ_1 ’s over the galactic halo in the present universe.¹ Each χ_1 then acquires a large Lorentz boost factor due to the mass gap between the two dark matter species.² Such boosted χ_1 scatters off material in the Earth to the unstable dark-sector state χ_2 , via a t -channel exchange of the dark gauge boson X . By construction, χ_2 is heavier than χ_1 , and hence decays back to χ_1 along with a quark pair whose hadronization eventually creates an EAS for the ANITA detector as long as the production happens in the atmosphere. In this scenario, the particle χ_1 behaves like a neutrino, as it is not only invisible but also ultra-relativistic, while the model parameters associated with χ_1 are relatively less constrained by existing experiments. Depending on the mass spectrum among χ_1 , χ_2 and X , either X or χ_2 can be naturally long-lived so that the quark pair $q\bar{q}$ can emerge in the atmosphere with a sizable probability. We shall discuss both of the possibilities in our analysis and demonstrate that they successfully accommodate the ANITA events, yielding the highest event probability at an emergence angle θ_{em} of $25^\circ - 35^\circ$ around which the two reported events are associated.

We additionally provide generic insights in order to understand the angular distribution of the events predicted for ANITA in the general case where a long-lived particle from the dark sector would be produced through scattering of a boosted dark-sector particle in the Earth and decay into hadronic final states in the atmosphere. In particular, we show that the situation where the mean free path of the boosted incoming particle is much larger than the Earth diameter but where its decay product has a mean decay length of dimensions comparable to the Earth radius can lead to an interesting “translucent” case in which the angular distribution can culminate at moderately large emergence angles.

The paper is structured as follows. In Sec. II we start by developing general arguments and demonstrate how the Earth transparency can help predicting events for ANITA with relatively large emergence angles. In

¹ In principle, $\phi \rightarrow \chi_1 + Y$ with Y collectively representing all other particles is possible, but we take $\phi \rightarrow \chi_1\chi_1$ as a benchmark model.

² Similar scenarios in which the decay of a heavier dark matter component boosts a pair of lighter dark matter components have been discussed in the context of explaining the IceCube PeV-neutrino events [19, 20].

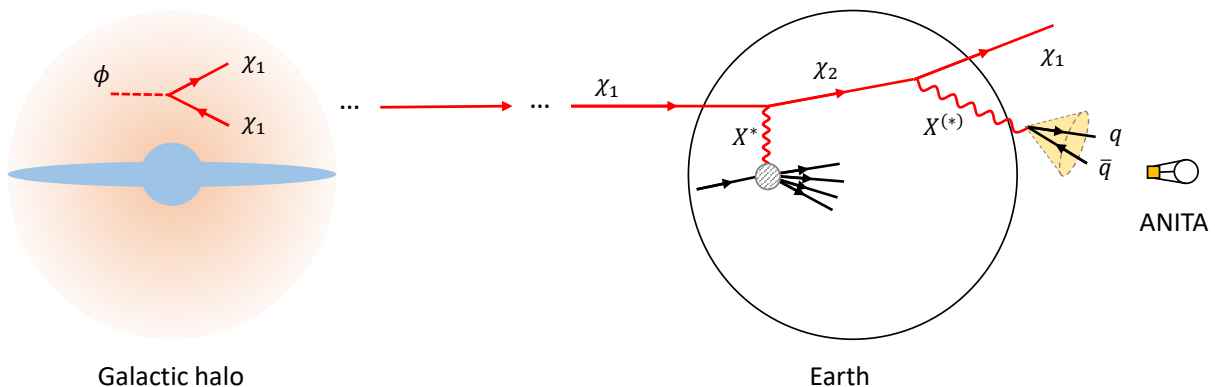


FIG. 1. The benchmark dark-matter scenario under consideration for explaining the ANITA anomaly. The travel lengths of individual particles and the angles between particles are randomly chosen for illustration; that is, they do not represent any ANITA-related events at all.

Sec. III, we define our benchmark model which may give rise to the signal of interest. Our analysis procedure including relevant Monte Carlo simulation is detailed in Sec. IV. We then report our main findings and results in Sec. V, followed by some discussions and interpretations. Section VI is reserved for conclusions and future prospects.

II. UNDERSTANDING THE ANGULAR DISTRIBUTION OF EAS

The ANITA Collaboration has thus far collected 85.5-day data for three different flights, and recorded more than 30 interesting events. Of them, 2 events are identified upward-moving with an energy of ~ 0.6 EeV, as they do not show a phase reversal characteristic of EAS. Hence, high-energetic upward-propagating cosmic rays may induce these events. Event specifications in terms of reconstructed energy E_{rec} and emergence angle θ_{em} are summarized below, while we refer to [1, 2] for more details.

- Event #3,985,267 in ANITA I: $E_{\text{rec}} = 0.6 \pm 0.4$ EeV and $\theta_{\text{em}} = 25.4 \pm 1^\circ$
- Event #15,717,147 in ANITA III: $E_{\text{rec}} = 0.56^{+0.3}_{-0.2}$ EeV and $\theta_{\text{em}} = 35.5 \pm 1^\circ$

One of the most puzzling features of these anomalous events, besides the propagation of very high-energy particles on large distances, is the angular distribution of such events. While most of the existing interpretations simply rely on the total effective area of the detector in order to compute a total number of events for a certain astrophysical flux, Refs. [9, 10, 15–17] have attempted to describe the angular repartition of the events predicted by an incoming flux of sterile/right-handed neutrinos. However, the distributions in these studies generically favor relatively small emergence angles ($\lesssim 10^\circ$), even though they provide an explanation for the number of events observed

by the ANITA Collaboration at angles larger than SM neutrinos would do.

In light of this phenomenological challenge, we discuss what class of scenarios would preferentially give rise to events with a relatively large emergence angle. As detailed in Sec. III, all the ingredients in our benchmark model, the incident particle arriving on the Earth, the particles propagating through the Earth, and the particle inducing an EAS in the low atmosphere, belong to a dark sector. In this section we shall develop some fairly model-independent insight about how the scenario of this sort can give rise to an angular distribution of EAS which is in favor of smaller or larger emergence angles recorded by ANITA. To this end, we simplify the situation at hand, assuming that a particle A scatters off a nucleon and produces a particle B which propagates through the Earth and decays into pairs of quarks:

$$A \xrightarrow{\sigma_{AN}} B \xrightarrow{\Gamma_B} \bar{q}q, \quad (2.1)$$

where σ_{AN} and Γ_B parameterize the scattering process of A and the decay of B , respectively. As described in more detail in Sec. IV, the effective area of the ANITA detector is a convolution of following different effects:

1. The bigger σ_{AN} is, the more B particles are produced inside the Earth for a given incoming flux of A . Thereafter, the longer-lived the B particle is, the more probable it decays after escaping the surface rather than inside the Earth.
2. Once escaping the Earth, the shorter-lived the B particle is, the more it decays before passing the ANITA detector.
3. Depending on the location of the decay and the opening angle between the ANITA detector and the shower axis, the resulting electric field may initiate detection of an event.

The effective area of the detector per unit emergence

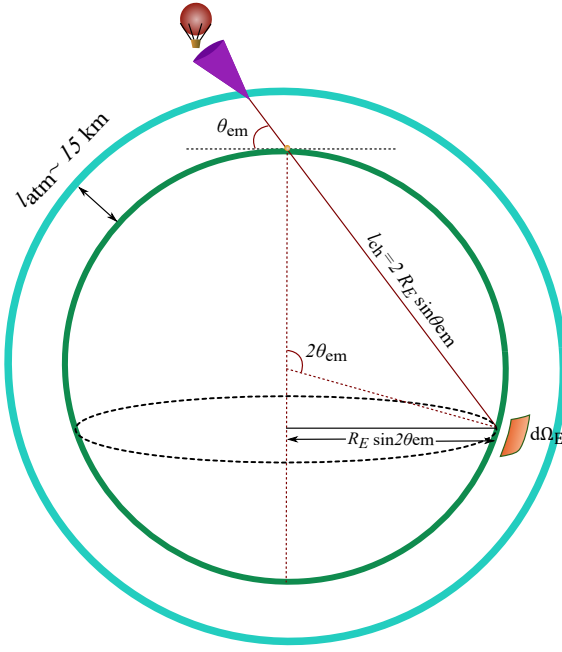


FIG. 2. Geometry of the chord propagation, as a function of the emergence angle θ_{em} . The chord propagation and the Earth radius join at an angle of $\pi/2 - \theta_{em}$.

angle can then be sketched to be of the form

$$dA_{\text{eff}} \approx d\Omega_E(\vec{r}_{\text{ch}}) \otimes P_{\text{ex}}(\theta_{\text{em}}, \mathcal{E}_{\text{ex}}) \otimes P_{\text{dec}}(\theta_{\text{em}}, \mathcal{E}_{\text{ex}}) \otimes P_{\text{det}}(\vec{r}_{\text{ch}}), \quad (2.2)$$

where \vec{r}_{ch} denotes the spatial direction of the chord of interest and where $d\Omega_E$ corresponds to the Earth elementary area per unit emergence angle (integrated over the azimuthal angle around the rotation axis of the Earth). The quantity $P_{\text{ex}}(\theta_{\text{em}}, \mathcal{E}_{\text{ex}})$ denotes the probability that a particle B escapes the Earth with an energy of \mathcal{E}_{ex} for a given incoming particle A (step 1.). Finally, $P_{\text{dec}}(\theta_{\text{em}}, \mathcal{E}_{\text{ex}})$ and $P_{\text{det}}(\vec{r}_{\text{ch}})$ respectively stand for the probability that the particle B decays in the atmosphere (step 2.) and the probability that the shower produced by such a decay is detected by ANITA (step 3.).

For simplicity, we assume for now that the detected showers are so boosted that we can consider only the chords crossing the ANITA location and simply look at the variation of these quantities as a function of the emergence angle only. In our scenario, the particles A and B are so feebly interacting that we can neglect any loss of energy which could arise while propagating. Therefore, the exit energy \mathcal{E}_{ex} can be uniquely related to the energy of the incoming A particle.

The elementary solid angle contributing to the effective area, integrated over the azimuthal angle, for a given emergence angle (see FIG. 2) is

$$R_E^2 d\Omega_E(\vec{r}_{\text{ch}}) = 4\pi R_E^2 \sin \theta_{\text{em}} \sin 2\theta_{\text{em}} d\theta_{\text{em}}, \quad (2.3)$$

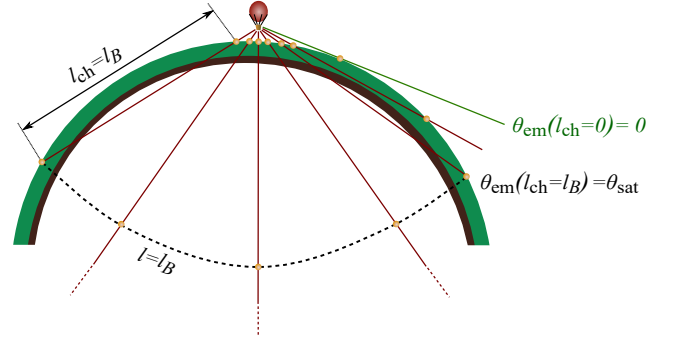


FIG. 3. Region of the Earth crust inside which the scattering of a feebly interacting particle A produces a particle B of decay length l_B which would have a significant probability to escape the Earth if propagating on a chord of length $l_{\text{ch}} \lesssim l_B$.

where R_E stands for the radius of the Earth. Therefore, neglecting the altitude of the ANITA radio-antenna, we see that a particle – which would ideally propagate freely through the Earth, decay in the low atmosphere with probability being one, and produce a sufficiently energetic EAS – would be detected by ANITA with a total effective area equal roughly to the Earth area, which is a strength of the ANITA detector. Obviously, Eq. (2.3) implies that the angular distribution of the events detected by ANITA would be necessarily suppressed around $\theta_{\text{em}} = 0^\circ$ and $\theta_{\text{em}} = 90^\circ$ while showing a peak at $\theta_{\text{em}} = 54.7^\circ$.

However, in the presence of interactions in the Earth, the interaction probability of the particle A along a chord of length l_{ch} varies as

$$\frac{dP_{\text{scat.}}}{dl}(l < l_{\text{ch}}) = \frac{1}{l_A} \exp\left(-\frac{l}{l_A}\right), \quad (2.4)$$

where l_A denotes the mean free path of A . This distribution sharply peaks around $l \ll l_{\text{ch}}$ in the case of $l_{\text{ch}} \gg l_A$, but becomes relatively flat in the case of $l_{\text{ch}} \ll l_A$. Therefore, the shorter l_A is, the more the scattering processes happen immediately after A enters the Earth surface.

In the former case (i.e., $l_{\text{ch}} \gg l_A$), the efficiency of the scattering process would then be almost independent of the emergence angle. Thereafter, if the particle B produced by such a scattering is long-lived enough, it would escape the Earth with a probability being higher at low emergence angles, since the probability that it decays inside the Earth is smaller for small propagation lengths as compared to particles produced deep under the surface. Such a scenario would therefore be disfavored by the fact that ANITA has seen anomalous events at relatively large emergence angles.

By contrast, in the latter case (i.e., $l_{\text{ch}} \ll l_A$), the Earth is almost transparent to the incoming particles so that the probability in Eq. (2.4) can be approximated to

$$\frac{dP_{\text{scat.}}}{dl_{\text{ch}}}(l < l_{\text{ch}}) \approx \frac{1}{l_A}. \quad (2.5)$$

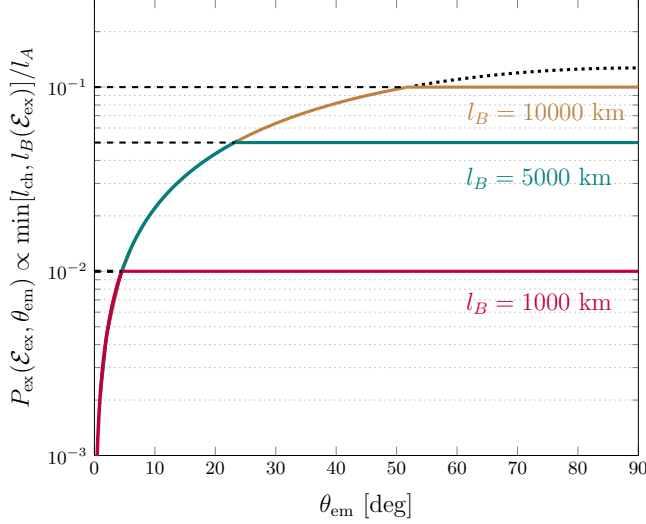


FIG. 4. Sketch of the shape of the exit probability function P_{ex} for $l_B \lesssim l_{\text{ch}} \ll l_A$, according to the piecewise function given in Eq. (2.7). l_A is fixed to 10^5 km for illustration. Shown are the cases with three representative values of the decay length l_B , one smaller than, one comparable to, and one larger than the Earth radius by purple, teal, and brown curves, respectively.

This implies that the interaction probability along a chord of l_{ch} is simply l_{ch}/l_A . If particle B is long-lived enough, then the exit probability becomes (roughly) proportional to $P_{\text{scat.}}$, i.e.,

$$P_{\text{ex}}(\theta_{\text{em}}, \mathcal{E}_{\text{ex}}) \propto \frac{l_{\text{ch}}}{l_A} \quad \text{for } l_A \gg l_{\text{ch}}, \quad (2.6)$$

and the relation is valid as far as the decay length of B is larger than the chord length. This shows that the resulting probability distribution is a linearly increasing function in l_{ch} or equivalently in θ_{em} .³ On the other hand, if particle B is relatively short-lived (i.e., its decay length is shorter than the chord length), the event where A scatters at a depth larger than the B decay length would not allow B to escape the Earth surface since it is likely to decay earlier. The volume of the Earth contributing efficiently to the production of B which may escape is therefore delimited by the surface $l = \min(l_{\text{ch}}, l_B)$ as depicted in FIG. 3. The exit probability is then scaling like

$$P_{\text{ex}}(\theta_{\text{em}}, \mathcal{E}_{\text{ex}}) \propto \frac{\min[l_{\text{ch}}, l_B(\mathcal{E}_{\text{ex}})]}{l_A} \quad \text{for } l_B \lesssim l_{\text{ch}}. \quad (2.7)$$

In other words, the proportionality of P_{ex} simply follows l_{ch} for $l_{\text{ch}} < l_B$ and is frozen to $l_{\text{ch}} = l_B$ for $l_{\text{ch}} > l_B$.

³ Note that the effect is accentuated as the mean density along the chord is larger when the chord length increases.

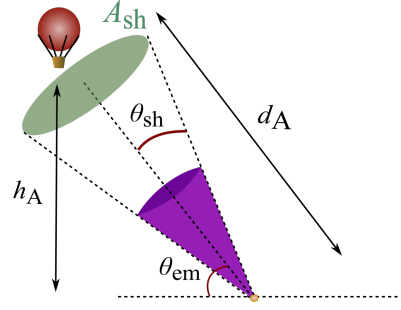


FIG. 5. Notational conventions for the geometry of the shower opening.

This implies that if the decay product is short-lived as compared to the radius of the Earth, the exit probability has to saturate to a constant value, independent of the emergence angle θ_{em} as is schematically shown in FIG. 4 with illustrative values of the decay length l_B .

As far as the decay probability is concerned, for a particle B escaping the Earth with an emergence angle θ_{em} , the probability that B decays before reaching an altitude $h_{\text{atm}} \sim 15$ km is given by

$$P_{\text{dec}}(\theta_{\text{em}}, \mathcal{E}_{\text{ex}}) = 1 - \exp\left(-\frac{l_{\text{atm}}(\theta_{\text{em}})}{l_B(\mathcal{E}_{\text{ex}})}\right), \quad (2.8)$$

where

$$l_{\text{atm}}(\theta_{\text{em}}) = -R_E \sin \theta_{\text{em}} + \sqrt{(R_E + h_{\text{atm}})^2 - R_E^2 \cos^2 \theta_{\text{em}}}. \quad (2.9)$$

Once the shower created in the lower atmosphere, with a maximum angular opening θ_{sh} , we assume that in our analysis ANITA can observe the signal as long as the detector is located inside the cone originating at the point of the decay, as depicted in FIG. 5. Therefore, the capability of detecting a shower, encoded in P_{det} for a given emergence angle, need to be weighted by the surface area of the shower A_{sh} at the detector location which is, in turn, quadratically proportional to the distance between the ANITA detector and the decay point d_A :

$$P_{\text{det}} \propto A_{\text{sh}} \propto d_A(\theta_{\text{em}})^2 = \left(-R_E \sin \theta_{\text{em}} + \sqrt{(R_E + h_A)^2 - R_E^2 \cos^2 \theta_{\text{em}}}\right)^2, \quad (2.10)$$

where $h_A (= 35 \text{ km})$ is the altitude of the ANITA detector above the Earth. However, the reader should note that if showers are emitted too far from the detector, the resultant electric field amplitude may be diminished and as a consequence the detector may not be triggered. A proper treatment for such an effect would require a careful simulation study on the shower electric field, which is beyond the scope of this work. Nevertheless, we expect that it would tend to suppress even more the effective

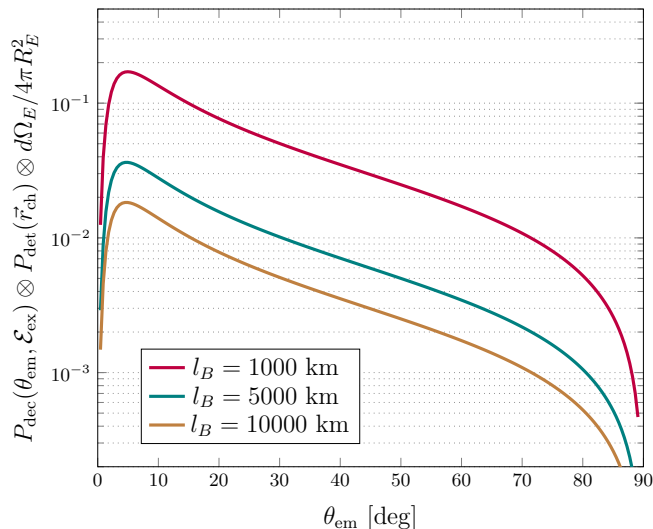


FIG. 6. Probability that an escaping B particle with emergence angle θ_{em} decays within 15 km of altitude, weighted by the detection probability $P_{\text{det}}(\vec{r}_{\text{ch}})$ and the elementary solid angle $d\Omega_E(\vec{r}_{\text{ch}})$, for the same choices of l_B as in FIG. 4.

area towards lower angles in favor large emergence angles, enhancing the effect that we are describing here.

In FIG. 6 we plot the differential probability, combining $P_{\text{dec}}(\theta_{\text{em}}, \mathcal{E}_{\text{ex}})$, $P_{\text{det}}(\vec{r}_{\text{ch}})$, and the elementary solid angle of Eq. (2.3). The functional behavior of the final effective area in θ_{em} is given in competition between the combined probability in FIG. 6 and the exit probability in FIG. 4. We now categorize various possibilities into three different regimes enumerated below.

- **Opaque case:** In the case, similarly to the SM neutrino one, where the Earth is opaque enough to absorb most of the B particles before they can escape the Earth, the exit probability is suppressed at large emergence angles (see also purple curves). Therefore, given the similar suppression of the decaying probability of B exhibited in FIG. 6, the effective area of ANITA will peak at a very small emergence angle.
- **Transparent case:** In the case where the Earth is transparent, both to the A particle and to the decaying particle B , the exit probability will basically be given by the evolution of the chord length (see also brown curves). As a consequence, it will be maximized at a large angle. The suppression of the decay probability will compete only at large emergence angles, leading to an overall shape of the effective area with a maximum relatively close to the vertical (i.e., $\theta_{\text{em}} = 90^\circ$).
- **Translucent case:** In the intermediate case, where the Earth would be relatively transparent to A but where B would have a decay length comparable to the Earth radius, the shape of the effective

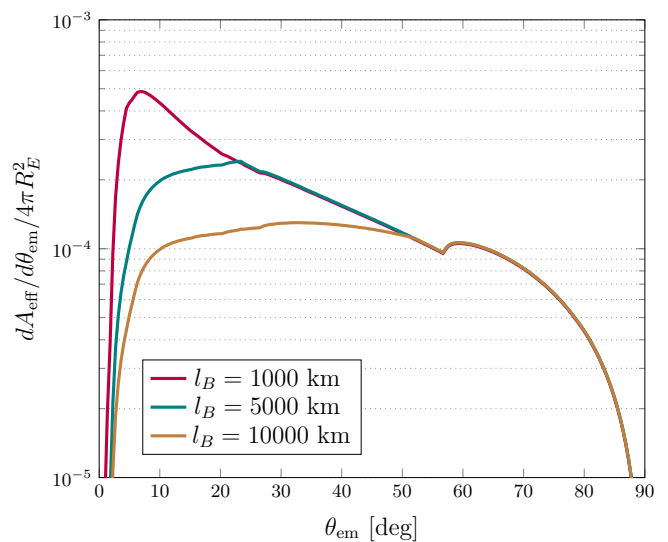


FIG. 7. Qualitative estimate for the effective area of the detector. l_A is fixed to 10^5 km and three different l_B values are chosen. For completeness, probability values are additionally weighted by the mean density along the chord, in order to incorporate the better scattering rate at large emergence angles due to the higher density of the Earth along the propagation.

area will possess the maximum at a value of the emergence angle around $25^\circ - 35^\circ$, which could potentially explain the value of the emergence angle of the anomalous events observed by the ANITA Collaboration (see also teal curves).

We also visualize this qualitative summary of the three regimes in FIG. 7, not only incorporating the different contributions to the effective area but taking into account the fact that different emergence angles are, in reality, affected by different mean density along the propagation chord $\langle \rho \rangle_{\text{ch}}$ (we used in our simulation the Preliminary Earth Reference Model of Ref. [21]). The latter factor essentially affects the exit probability P_{ex} . We simply re-weight it by $\langle \rho \rangle_{\text{ch}} / \rho_{\text{max}}$ with ρ_{max} being the maximum density inside the Earth as we are here interested in spectral behaviors of A_{eff} . From now on we explore a model of inelastic boosted dark matter, and show that viable regions of parameter space can describe the above-discussed translucent case.

III. BENCHMARK MODEL

We are now in the position to define our benchmark dark-matter model to explain the ANITA anomaly. Once the model definition is established, we discuss production of boosted dark matter followed by its expected flux near the Earth in the first subsection. The next subsection focuses on the scattering of the boosted dark matter in the Earth to create a long-lived particle. Finally, a detailed

discussion on the decay of the long-lived particle appears in the last subsection.

A. Benchmark model and production of boosted dark matter

As briefly mentioned in the Introduction, the minimal particle contents include super-heavy dark matter ϕ , light dark matter χ_1 , dark-sector unstable state χ_2 , and dark gauge boson X . For simplicity, we assume that ϕ is scalar while $\chi_{1,2}$ are Dirac-fermionic. The interaction Lagrangian \mathcal{L}_{int} contains the following operators:

$$\mathcal{L}_{\text{int}} \supset y_\phi \phi \bar{\chi}_1 \chi_1 \quad (3.1)$$

$$-\frac{\epsilon}{2} F_{\mu\nu} X^{\mu\nu} + (g_{12} \bar{\chi}_2 \gamma^\mu \chi_1 X_\mu + \text{h.c.}), \quad (3.2)$$

where $X_{\mu\nu}$ ($F_{\mu\nu}$) is the field strength tensor for the dark gauge boson X (the ordinary SM photon) and ϵ is the usual kinetic mixing parameter. The term in (3.1) governs the decay of ϕ to a χ_1 pair and a Yukawa coupling y_ϕ parameterizes the decay strength.⁴ On the other hand, the second term in (3.2) takes care of the up-scattering process of χ_1 to χ_2 and the decay of χ_2 to χ_1 and X , with g_{12} encoding their strength.

We emphasize that in the above model the heavier dark matter species ϕ does not have direct couplings to SM particles, whereas the lighter one χ_1 has direct interactions through a dark gauge boson portal. Therefore, any loop-induced decay modes of ϕ to SM particles are suppressed enough for ϕ to predominantly decays to a pair of χ_1 's.

Speaking of dark matter relics, we assume that ϕ dominates over χ_1 , so the dark-matter halo in our galaxy essentially consists of ϕ . Be aware that the ϕ dominance is, in principle, not a necessary condition to explain the ANITA events. The reduction of the ϕ fraction would decrease the flux of χ_1 linearly, but it can be compensated by lessening the lifetime of ϕ (as shown in Eq. (3.4)) as far as such a trade-off is consistent with various astrophysical and cosmological observations. We further imagine the situations where the mass of χ_1 , m_1 is of MeV to GeV-range, so it can be thermally produced in the early universe. The present-day relic density of such χ_1 is determined by interrelationships among ϵ , m_1 , and

the mass of dark gauge boson m_X . The relic of χ_1 can be subdominant in a wide range of parameter space as long as $m_1 > m_X$ (and in the resonance regime $2m_1 \simeq m_X$), and therefore our aforementioned assumption is readily satisfied. On the other hand, EeV-scale super-heavy ϕ under consideration is produced non-thermally [23, 24], and it is possible for such ϕ to take care of almost entire relic abundance of cold dark matter.

Since relic dark matter is mostly given by ϕ , it is reasonable to assume that the spatial distribution of ϕ obeys standard dark matter halo density distributions. Our choice in this study is the Navarro-Frenk-White profile [25, 26], so the ϕ energy density ρ_ϕ has the form of

$$\rho_\phi(r) = \rho_0 \frac{(r/r_s)^{-1}}{(1 + r/r_s)^2}, \quad (3.3)$$

where $\rho_0 \simeq 0.3 \text{ GeV/cm}^3$ is the local dark-matter density at $r \simeq 8.33 \text{ kpc}$ and where $r_s = 24 \text{ kpc}$ is the scale radius. The flux of boosted dark matter χ_1 , \mathcal{F}_1 , for a given direction is then expressed as follows:

$$\mathcal{F}_1(\theta_d, \phi_{ra}) = \frac{2}{4\pi} \int_{\text{los}} ds \frac{1}{\tau_\phi} \cdot \left(\frac{\rho_\phi[r(s, \theta_d, \phi_{ra})]}{m_\phi} \right) \quad (3.4)$$

where τ_ϕ (or equivalently the inverse of decay rate Γ_ϕ) is the mean lifetime of ϕ and where the prefactor 2 takes into account the fact that ϕ decays to a pair of χ_1 's. Here the incident direction is parameterized by the declination angle θ_d and the right-ascension angle ϕ_{ra} in the International Celestial Reference System (ICRS). We remark that the radial coordinate r in ρ_ϕ is a function of these angles and the line-of-sight s , and so is the dark-matter energy density ρ_ϕ .

B. Scattering-off of boosted dark matter

Once such a boosted χ_1 reaches the Earth, it may scatter off a nucleon via a t -channel exchange of dark gauge boson X and a dark-sector unstable state χ_2 comes out. The nucleon usually breaks up due to a large energy transfer, so the process is essentially initiated with deep inelastic scattering (DIS) between χ_1 and nucleon N . The DIS of this sort is extensively explored in Ref. [27], and we simply quote their final result for $\sigma_{\chi_1 N}^{\text{DIS}}$:

$$\frac{d^2 \sigma_{\chi_1 N}^{\text{DIS}}}{dx dy} = \frac{\alpha \epsilon^2 g_{12}^2 f(x)}{2E_1(Q^2 + m_X^2)^2} \{ 2E_1^2 m_N x (2 - 2y + y^2) - m_N x (m_1 - m_2)^2 + [(m_1^2 - m_2^2)(2 - y) - 2m_1 m_2 y - 2m_N^2 x^2 y] E_1 \}, \quad (3.5)$$

where m_N denotes the nucleon mass of interest, α is the usual fine structure constant, and $f(x)$ is the associated parton distribution function (PDF). The relations among a dimensionful quantity Q^2 and two dimensionless quan-

⁴ To ensure sufficient stability of ϕ , y_ϕ should be extraordinarily small. The clockwork mechanism may generate dynamically such a tiny coupling constant [22].

ties x and y are given by

$$Q^2 = -(p_1 - p_2)^2, \quad (3.6)$$

$$y = 1 - \frac{E_2}{E_1}, \quad (3.7)$$

$$x = \frac{Q^2}{2m_N E_1 y}, \quad (3.8)$$

where p_1 and p_2 denote four momenta of the incoming χ_1 and the outgoing χ_2 , respectively. x implies the momentum fraction carried by a parton while y is fractional energy loss.

For a given E_1 one can calculate numerically the χ_1 -nucleon DIS cross sections, convolving relevant PDFs. In our analysis we model the total DIS cross section for a convenient parameter survey, after calculating $\sigma_{\chi_1 N}^{\text{DIS}}$ of several representative parameter points with MSTW2008NNLO [28]. We find that the following model describes functional behaviors of $\sigma_{\chi_1 N}^{\text{DIS}}$ in $0.1 \text{ EeV} \lesssim E_1 \lesssim 10 \text{ EeV}$ and $m_X \lesssim 10 \text{ GeV}$ fairly well:

$$\begin{aligned} \sigma_{\chi_1 N}^{\text{DIS}} &\approx 2.89 \times 10^{-29} \text{ cm}^2 \\ &\times \epsilon^2 g_{12}^2 10^{K(\log_{10}[m_X/\text{GeV}])} \cdot \left(\frac{E_1}{5 \text{ EeV}} \right)^{1.05}, \end{aligned} \quad (3.9)$$

where $K(x)$ has the form of

$$K(x) = -0.349x^3 - 0.452x^2 - 0.205x. \quad (3.10)$$

Note that the above empirical model does not depend on m_1 and m_2 . This is because our numerical study suggests that the variation in $\sigma_{\chi_1 N}^{\text{DIS}}$ be of order (at most) 2 – 3% with $m_{1,2} \lesssim 5 \text{ GeV}$. As we shall show in Sec. V, some parameter choices belonging to these ranges look highly plausible in generating ANITA-like events. So, we slenderize our parameter survey, relying on the above-given model and focusing on the associated parameter regions.

Given the cross section, one can estimate the mean free path of χ_1 . Kinetic theory suggests that the average travel distance of χ_1 (henceforth denoted by L_1 should be

$$L_1 \sim \frac{1}{\langle n(\theta_{\text{em}}) \rangle \cdot \sigma_{\chi_1 N}^{\text{DIS}}}, \quad (3.11)$$

where $\langle n \rangle$ is the mean nucleon number density along the χ_1 propagation chord. Since it depends on Earth layers that χ_1 traverses, we explicitly express its dependence on the emergence angle θ_{em} . Certainly, the functional behavior of $\langle n \rangle$ in θ_{em} is highly nontrivial, as the associated density profile inside the Earth shows a drastic change especially at the boundary between adjacent interior layers. Just to build up our intuition, we find that

$$\begin{aligned} L_1 &\approx 143,000 \text{ km} \left(\frac{10^{-3}}{\epsilon} \right)^2 \left(\frac{1}{g_{12}} \right)^2 \\ &\times 10^{-K(\log_{10}[m_X/\text{GeV}])} \cdot \left(\frac{5 \text{ EeV}}{E_1} \right)^{1.05} \end{aligned} \quad (3.12)$$

for $\theta_{\text{em}} = 30^\circ$ at which the chord length is the same as the Earth radius.

C. Decay of a long-lived particle

Once χ_2 is created, it decays back to χ_1 together with hadrons (through a quark pair) which invoke EAS. As mentioned in the Introduction, the χ_2 decay takes place via either on-shell or off-shell dark gauge boson, depending on the mass relation among χ_1 , χ_2 and X . Labeling them by “on-shell” scenario and “off-shell” scenario respectively, we discuss their characteristic features separately.

On-shell scenario: In this scenario m_2 is greater than $m_1 + m_X$ so that an on-shell X comes out as a decay product of χ_2 . Unless the coupling g_{12} and/or a mass gap $m_2 - m_1 - m_X$ is unusually small, the χ_2 decay is prompt (i.e., it occurs at the scattering point), and X may be long-lived and propagating. The total decay width of X , Γ_X is given by

$$\Gamma_X = \frac{\epsilon^2 \alpha m_X}{3} \sum_i C_i \left(1 + \frac{m_i^2}{m_X^2} \right) \sqrt{1 - \frac{4m_i^2}{m_X^2}}, \quad (3.13)$$

where C_i denotes the color factor for particle species i which runs over all charged SM fermions lighter than half the mass of X .⁵ As a rough estimate we see that the laboratory-frame mean decay length of X , $\ell_{X,\text{lab}}$ is

$$\ell_{X,\text{lab}} \sim 400 \text{ km} \left(\frac{10^{-5}}{\epsilon} \right)^2 \left(\frac{500 \text{ MeV}}{m_X} \right)^2 \left(\frac{E_X}{\text{EeV}} \right), \quad (3.14)$$

with E_X being the amount of energy that X carries.

One possible issue with this scenario is disappearance of X via $X + N \rightarrow \text{anything}$, before it decays. To develop some intuition on such a possibility, its cross section should be first estimated. If X is energetic enough to be treated nearly massless, we can get some hint from the photon-nucleon DIS cross section. From the experimental measurements of $\sigma_{\gamma p}^{\text{DIS}}$ at HERA [29, 30] we find

$$\sigma_{Xp}^{\text{DIS}} \approx 1.65 \times 10^{-36} \text{ cm}^2 \left(\frac{\epsilon}{10^{-4}} \right)^2 \left(\frac{E_{\text{c.o.m.}}}{200 \text{ GeV}} \right)^{0.22}, \quad (3.15)$$

where $E_{\text{c.o.m.}}$, the center-of-mass energy of the X - p system, is given by $\sqrt{2E_X m_p}$.⁶ One may estimate the typical distance for a single scattering process using the relation in (3.11), and see that the distance is much larger

⁵ A special care must be taken for quarks. Since hadrons appear as decay products, their masses, not quark ones, should be considered accordingly.

⁶ In Ref. [30] the exponent upon $E_{\text{c.o.m.}}$ is extracted with data for $E_{\text{c.o.m.}} \sim 200 - 300 \text{ GeV}$. We assume that this functional behavior does not alter much at $(2 \cdot 10^9 \text{ GeV} \cdot 1 \text{ GeV})^{1/2} \approx 45 \text{ TeV}$.

than the mean decay length above for a given set of E_X and ϵ . In other words, dark gauge boson is strongly inclined to decay before disappearing.

Off-shell scenario: Contrary to the previous scenario, the mass of dark gauge boson X is larger than the mass difference between χ_2 and χ_1 . Therefore, if the mass gap $\delta m (\equiv m_2 - m_1)$ (kinematically) allows for opening decay modes to SM fermion pairs, the associated decay process occurs via an off-shell X . χ_2 is now long-lived and the associated decay width Γ_2 is formulated [31] by the form of

$$\Gamma_2 \approx \frac{\epsilon^2 \alpha g_{12}^2}{15\pi^2 m_X^4} (\delta m)^5 \sum_i C_i, \quad (3.16)$$

under the assumption of $m_i \ll \delta m \ll m_2 \ll m_X$ (see Appendix B in Ref. [31] for the exact formula). Our rough estimate shows that the laboratory-frame mean decay length of χ_2 , $\ell_{2,\text{lab}}$ is

$$\ell_{2,\text{lab}} \sim 12,500 \text{ km} \left(\frac{10^{-4}}{\epsilon} \right)^2 \left(\frac{1}{g_{12}} \right)^2 \times \left(\frac{m_X}{2 \text{ GeV}} \right)^4 \left(\frac{0.5 \text{ GeV}}{\delta m} \right)^5 \left(\frac{\text{GeV}}{m_2} \right) \left(\frac{E_2}{\text{EeV}} \right), \quad (3.17)$$

where E_2 is the energy of the scattered χ_2 .

We close this section, rendering a few comments. It is summarized that the event topology under consideration begins with an upscattering of an invisible particle and accompanies a long-lived intermediary state decaying to hadrons. Indeed, the structure of upscatter-decay has been adopted in a diverse range of astrophysical phenomena [32–36], search strategies in particle accelerator experiments [37–44], double-bang events at IceCube [45, 46] and inelastic boosted dark matter [27, 31, 47, 48]. In particular, Refs. [49–51] have considered the up-scattering of dark matter to an excited state somewhere outside a detector, followed by its de-excitation in the detector along with visible particles. In the context of the ANITA anomaly, Refs. [13, 17] have taken related strategies.

IV. ANALYSIS PROCEDURE

In this section, we detail the procedure that we used in order to compute the differential number of events per emergence angle at which the ANITA detector would observe events according to our model prediction, redefining notation and conventions more carefully if needed. Generically, the expected number of signal events N_{sig} is given by the exposure time t_{exp} times the inner product of flux and effective area vectors. From Eq. (3.4) we see that our signal flux varies with the angles θ_d and ϕ_{ra} (see also FIG. 8 for the notations).⁷ Labeling the “effective”

area projected onto the flux vector by \mathcal{A}_{eff} , we remark that \mathcal{A}_{eff} potentially depends on θ_d and ϕ_{ra} . Therefore, N_{sig} is obtained after integrating over the incoming flux direction θ_d and ϕ_{ra} :

$$N_{\text{sig}} = t_{\text{exp}} \times \int d\Omega_{\text{ICRS}} \mathcal{A}_{\text{eff}}(\theta_d, \phi_{ra}) \mathcal{F}_1(\theta_d, \phi_{ra}), \quad (4.1)$$

where $d\Omega_{\text{ICRS}} = d(\cos\theta_d)d\phi_{ra}$. Note that in our model the energy of the incoming boosted dark-matter state, E_1 , is uniquely determined by the mass of the heavy dark-matter state ϕ . Therefore, the flux of χ_1 particles, \mathcal{F}_1 , is implicitly depending on E_1 . Likewise, (as we will see later) \mathcal{A}_{eff} varies with E_1 , so N_{sig} is essentially a function of the energy E_1 . For brevity, we will omit the E_1 dependence in what follows, unless it is necessary for a better understanding. We further note that for a given energy E_1 the effective area differs according to the emergence angle θ_{em} with which the decaying particle (either X or χ_2) escapes the surface of the Earth and according to its energy \mathcal{E}_{ex} when it exits the Earth crust. Therefore, for a given direction of the flux arrival (θ_d, ϕ_{ra}) , the effective area $\mathcal{A}_{\text{eff}}(\theta_d, \phi_{ra})$ can be formulated as

$$\mathcal{A}_{\text{eff}}(\theta_d, \phi_{ra}) = \int d\theta_{\text{em}} d\mathcal{E}_{\text{ex}} A_{\text{eff}}(\theta_d, \phi_{ra}; \theta_{\text{em}}, \mathcal{E}_{\text{ex}}), \quad (4.2)$$

where

$$A_{\text{eff}}(\theta_d, \phi_{ra}; \theta_{\text{em}}, \mathcal{E}_{\text{ex}}) \equiv \frac{d^2 \mathcal{A}_{\text{eff}}(\theta_d, \phi_{ra})}{d\theta_{\text{em}} d\mathcal{E}_{\text{ex}}}. \quad (4.3)$$

Since one of the main goals in our work is to obtain an appropriate angular distribution of the signal as seen by ANITA, we seek to obtain the differential number of signal events in θ_{em} , i.e.,

$$\frac{dN_{\text{sig}}}{d\theta_{\text{em}}} = t_{\text{exp}} \int d\Omega_{\text{ICRS}} d\mathcal{E}_{\text{ex}} A_{\text{eff}}(\theta_d, \phi_{ra}; \theta_{\text{em}}, \mathcal{E}_{\text{ex}}) \mathcal{F}_1(\theta_d, \phi_{ra}). \quad (4.4)$$

The key quantity in order to compute this angular distribution is the elementary effective area A_{eff} in Eq. (4.3) per emergence angle θ_{em} and exit energy \mathcal{E}_{ex} for a given direction $d\tilde{\Omega}_{\text{ICRS}}$ and energy E_1 of the incoming flux of χ_1 particles. This area essentially encodes all the dynamical details of the detection, from the χ_1 entrance in the Earth, its propagation and conversion into a long-lived state, to the possible decay of the latter in the atmosphere and the EAS detection by the radio-antennas of ANITA. Inspired by the analysis scheme in Ref. [4], we modulate the whole calculational procedure in the following fashion: for a given incoming energy and direction of the flux, we

⁷ Note, however, that the flux producing upward-going showers at the south pole corresponds to the decay of DM particle decaying

in the outskirts of the galaxy. Therefore the angular distribution of the incoming flux is essentially isotropic in our case. The impact of the choice of DM profile is therefore negligible in our work.

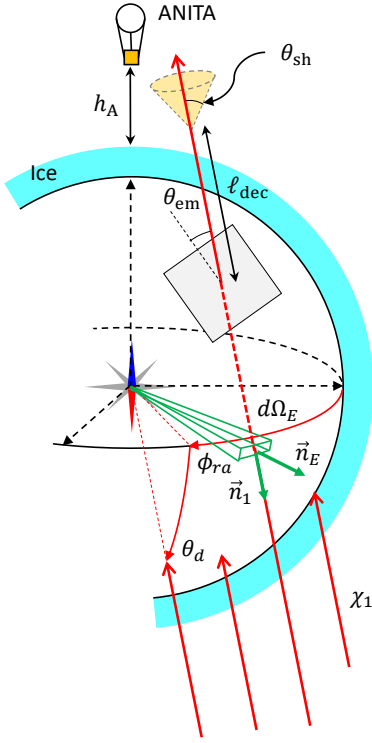


FIG. 8. The notation adopted in our simulation study.

- (i) integrate over the entire Earth surface, scanning over all the surface points of impact where a flux of χ_1 particles arriving along parallel chords strikes;
- (ii) compute the probability that the χ_1 propagates through the Earth, scatters and creates a long-lived particle (either X or χ_2) which escapes the Earth surface with a given energy \mathcal{E}_{ex} ;
- (iii) compute the probability that the long-lived particle decays in the atmosphere at a relevant height, creating an EAS;
- (iv) calculate the probability that such shower is detected by ANITA.

Such decomposition can be formulated as

$$\begin{aligned}
 A_{\text{eff}}(\theta_d, \phi_{ra}; \theta_{\text{em}}, \mathcal{E}_{\text{ex}}) = & \\
 & R_E^2 \int d\Omega_E \vec{n}_E \cdot \vec{n}_1 \quad \text{for (i)} \\
 & \times \frac{d}{d\mathcal{E}_{\text{ex}}} P_{\text{ex}}(E_1; \theta_d, \phi_{ra}; \theta_{\text{em}}, \theta_E, \phi_E) \quad \text{for (ii)} \\
 & \times \int d\ell_{\text{dec}} \frac{dP_{\text{dec}}(\mathcal{E}_{\text{ex}})}{d\ell_{\text{dec}}} \quad \text{for (iii)} \\
 & \times P_{\text{det}}(\mathcal{E}_{\text{EAS}}, \theta_{\text{sh}}, \ell_{\text{dec}}; \theta_d, \phi_{ra}; \theta_E, \phi_E), \quad \text{for (iv)}
 \end{aligned} \tag{4.5}$$

where \vec{n}_E is the Earth-surface unit normal vector while \vec{n}_1 is a unit vector lying in the flux direction of χ_1 (see also FIG. 8). The solid angle element with respect to the

Earth center is denoted by $d\Omega_E = d(\cos\theta_E)d\phi_E$. In the third row we explicitly express the dependence of the differential exit probability $dP_{\text{ex}}/d\mathcal{E}_{\text{ex}}$ on E_1 as well. In the fourth row the decay probability of the long-lived particle is integrated along its propagation chord. Finally, in the last row P_{det} describes the capability for a given EAS to yield a sufficient electric field along a direction which would reach the payload hence result in detection. We mark its dependence on the shower opening angle θ_{sh} and the energy of EAS \mathcal{E}_{EAS} . The ensuing subsections are devoted to discussing in more details the calculation of the steps (ii) through (iv).

A. Exit probability

Throughout this work, we perform a Monte Carlo simulation in order to estimate accurately the exit probability P_{ex} appearing in the third row of Eq. (4.5), as a function of the emergence angle θ_{em} . To this end, we adapted the public code provided with Ref. [52] for our BSM scenario. Assuming the Earth surface to be covered by a 4 km-thick ice layer, the simulation accounts for the varying density of the Earth crust along the propagation chord.

The quantity $dP_{\text{ex}}(E_1; \theta_d, \phi_{ra}; \theta_{\text{em}}, \theta_E, \phi_E)/d\mathcal{E}_{\text{ex}}$ is defined as the probability that an incoming boosted dark-matter particle χ_1 – which arrives with an incidence angle θ_i (corresponding to an emergence angle $\theta_{\text{em}} = 90^\circ - \theta_i$) and an energy E_1 – exits the Earth with an energy \mathcal{E}_{ex} . For every emergence angle θ_{em} , each event of the Monte Carlo simulation therefore tracks along the propagation chord the different possible interactions, according to the two aforementioned benchmark scenarios.

On-shell scenario:

1. An incoming χ_1 particle scatters off a nucleon with the cross-section appearing in Eq. (3.9) and converts into a particle χ_2 which promptly decays into a dark photon X and a boosted particle χ_1 ,
2. the dark photon X propagates until it reaches the Earth surface, as long as it does not decay inside the Earth, and
3. the (secondary) boosted dark-matter particle χ_1 produced by the χ_2 decay propagates until it re-scatters inside the Earth or escapes the surface.

Off-shell scenario:

1. An incoming χ_1 particle scatters off a nucleon with the cross-section shown in Eq. (3.9) and converts into particle χ_2 ,
2. the dark-sector particle χ_2 propagates until it decays inside the Earth or escapes the surface, and
3. in the case that χ_2 decays inside the Earth, its decay product (secondary) χ_1 propagates until it re-scatters inside the Earth or escapes the surface.

Pursuing the propagation of secondary χ_1 's created in the Earth by the χ_2 decay allows us to keep track of possible regeneration which could potentially increase the exit probability at large emergence angles and low exit energies. However, our simulation study suggests that the regeneration play an insignificant role in the scenarios that we investigate in this work, as we have elaborated in Sec. II. We therefore focus on cases where the Earth is relatively transparent to the flux of incoming particles.

B. Decay probability in the atmosphere

Once a long-lived particle species i ($= X$ or χ_2) comes out of the Earth surface, its decay simply obeys the exponential decay law

$$\frac{dP_{\text{dec}}(\mathcal{E}_{\text{ex}})}{d\ell_{\text{dec}}} = \frac{1}{\ell_{i,\text{lab}}} e^{-\ell_{\text{dec}}/\ell_{i,\text{lab}}}, \quad (4.6)$$

where $\ell_{i,\text{lab}}$ is the laboratory-frame mean decay length of the long-lived particle i . In the two cases where $i = X$ and $i = \chi_2$, the results appearing in Eqs. (3.14) and (3.17) can be substituted to $\ell_{i,\text{lab}}$ with E_X and E_2 replaced by \mathcal{E}_{ex} .⁸

As shown in Ref. [15], in the case where an astrophysical flux would produce tau leptons inside the Earth, the exit probability of the tau leptons would spread over a wide range of exit energies. Indeed, taus quickly lose energy while propagating in the Earth. Moreover, during regeneration processes, the particle produced through a decay, which may then re-scatter off a nucleon, will lead to an event with even lower exit energy. In our case, this sort of energy loss of the particles propagating through the Earth can be negligible since their interactions with the visible sector particles are very feeble. We therefore take into consideration only the energy losses (with respect to incoming energy E_1), which are caused by the fractional energy release in the scattering and decay processes.

The value of the exit energy has a crucial impact on the decay probability since the more boosted particles are, the less they are expected to decay before reaching the ANITA detector. Our simulation carefully takes care of possible energy diminishment down to $\mathcal{E}_{\text{ex}} = 100$ TeV, although most of the events involve a much larger exit energy in our proposed model due to the reasons discussed above.

C. Detection probability

The hadronic decay products can create an EAS in the atmosphere which can eventually be detected by

the radio-antennas of ANITA at an altitude of $h_A \sim 35$ km. Experimentally, it is not sufficient that the shower reaches the payload but the local electric field measured by the ANITA detector should be large enough to overcome the associated threshold. Here the probability P_{det} parameterizes the likelihood of recording an event with such effects considered.

The authors of Ref. [4] have performed a dedicated analysis regarding this probability, drawing a few important observations: (a) it gets gradually challenging for a shower created at altitudes above $\mathcal{O}(10)$ km to induce a fully-developed EAS, (b) the electric field peak, depending on the altitude where the shower is produced, lies at an opening angle θ_{sh} in-between $\sim 1^\circ$ and $\sim 2^\circ$, (c) the lower \mathcal{E}_{ex} is, the less the ANITA detector is triggered, and (d) the further from the ANITA detector the EAS is produced, the less likely it is to be detected.

Unfortunately, although Ref. [4] provides an approximate formula in order to evaluate the electric field produced by an EAS at the ANITA location, with an emergence angle of 30° and arbitrary distance from the point of decay and shower angle, the exact functional dependence of the parameters involved in this expression with the emergence angle has not been exhibited. This renders the evaluation of the precise probability P_{det} challenging from a theoretical point of view. For simplicity, we rather use the main conclusions of Ref. [4], following the assumptions made in Ref. [15], that is, we assume that $P_{\text{det}} = 1$ as long as the shower is produced at an altitude lower than 15 km, and whenever the detector is contained in a cone of angular opening $\theta_{\text{sh}} < 1.5^\circ$ with respect to the shower axis, and $P_{\text{det}} = 0$ otherwise.

Finally, the \mathcal{E}_{EAS} dependence of P_{det} must be taken with care, as the energy of the EAS could potentially be related to \mathcal{E}_{ex} in a non-trivial manner. In the “on-shell” scenario, the whole energy of the escaping X is transferred to decay products as it decays fully visibly. Therefore, we are allowed to set $\mathcal{E}_{\text{EAS}} = \mathcal{E}_{\text{ex}}$. On the contrary, in the “off-shell” scenario, a certain fraction of \mathcal{E}_{ex} is taken away by the outgoing χ_1 . We find that if $\chi_{1,2}$ are sufficiently heavier than hadronic decay products, χ_1 is produced nearly at rest in the χ_2 rest frame. Therefore, in the laboratory frame, χ_1 takes away $\sim (m_1/m_2)\mathcal{E}_{\text{ex}}$, and our simulation study with PYTHIA 8 [53] confirms that a large majority of events conforms to this estimate. In our analysis with off-shell scenario, we survey parameter space satisfying such mass relations, and thus adopt the approximation that $\mathcal{E}_{\text{EAS}} \approx (\delta m/m_2)\mathcal{E}_{\text{ex}}$.

V. RESULTS AND INTERPRETATIONS

We now report our simulation results in this section, followed by discussing their phenomenological implications. In order to demonstrate that the inelastic boosted dark matter scenario can accommodate the ANITA anomalous events, we choose the following two benchmark sets of parameters for the on-shell and off-

⁸ Be aware again that Eq. (3.17) is an approximation valid under restricted mass spectra. Our simulation study was based on the exact formula in Ref. [31].

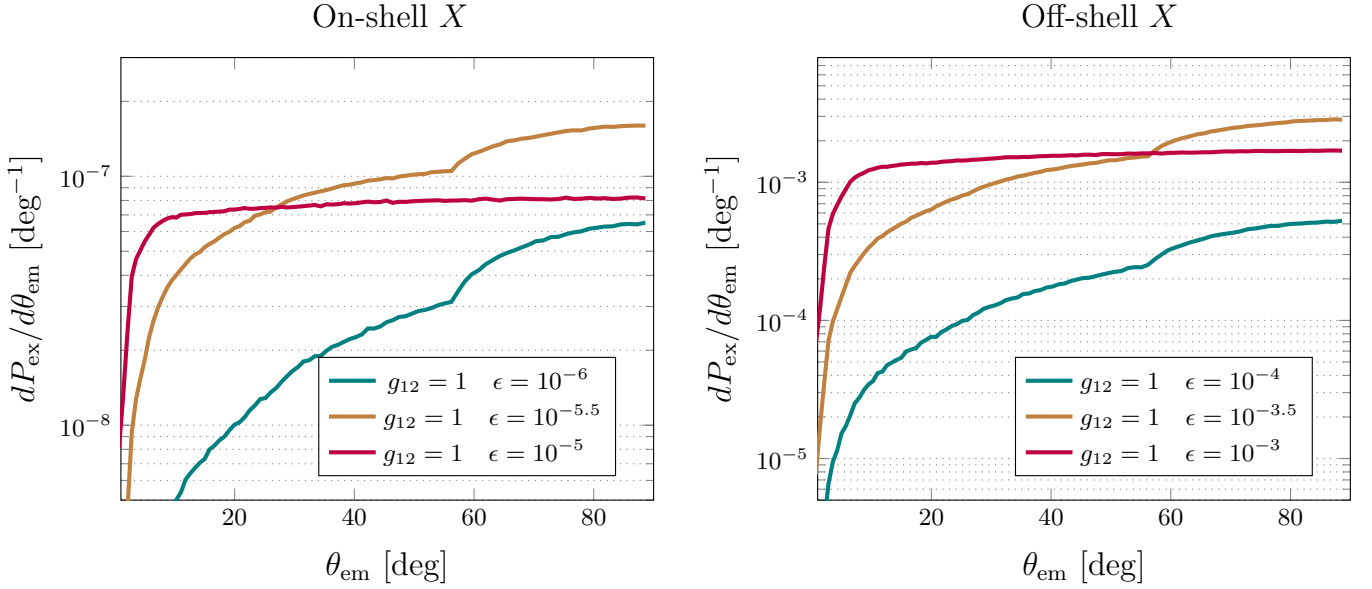


FIG. 9. \mathcal{E}_{ex} -integrated differential exit probability in emergence angle θ_{em} for the “on-shell” scenario (left panel) and the “off-shell” scenario (right panel). Mass parameter choices are summarized in (5.1), while the values of coupling constants ϵ and g_{12} are displayed in the legends.

shell cases.

On-shell: $m_2 > m_1 + m_X$, $m_X = 0.5$ GeV,
 $m_\phi = 2$ EeV,

Off-shell: $m_2 = 2.5$ GeV, $m_1 = 2$ GeV, $m_X = 2$ GeV,
 $m_\phi = 4$ EeV. (5.1)

Note that in the on-shell case the masses of χ_1 and χ_2 do not play any role either in the simulation of the effective area or in the decay width of the dark gauge boson, as long as they satisfy the mass relation with X , they are light enough to be considered relativistic, and χ_2 decays instantly. By contrast, in the off-shell scenario, all the mass values affect the propagation and the decay, although m_1 does not play a role in the propagation code. The m_ϕ values are selected in such a way that the associated hadronic decay products collectively carry away an energy within $0.5 - 1$ EeV.

In FIG. 9 we exhibit the differential exit probability in the emergence angle θ_{em} , integrating over all possible exit energy \mathcal{E}_{ex} . The left and right panels correspond to the on-shell and off-shell scenarios, respectively, for which we vary the value of the kinetic mixing parameter ϵ with the value of the dark-sector coupling g_{12} fixed to unity. We see that the red curves in both scenarios show a different behavior from the others. As we elaborated in Sec. II, this is because the mean decay length of X (for the on-shell scenario in the left panel) or χ_2 (for the off-shell scenario in the right panel) resulting from the associated parameter choices is much shorter than most of the chord lengths so that the exit probability quickly saturates in increasing θ_{em} .

We remark that the variation in g_{12} would alter the

results in FIG. 9 in different manners in the on-shell and off-shell scenarios. In the former case, raising g_{12} would result in enhancing the scattering cross section, while the decay length of X remains unaffected. As far as the mean free path of χ_1 keeps much larger than the dimension of the Earth, this would simply lead the effect of rescaling the total exit probability by g_{12}^2 . On the contrary, in the latter case, both the scattering cross section and the decay width of χ_2 scale as $g_{12}^2 \epsilon^2$. Therefore, increasing or decreasing the dark-sector coupling is equivalent to inversely varying the kinetic mixing parameter by the same magnitude.

Following the procedure described in Sec. IV, we next integrate over the incoming χ_1 directions defined by the (θ_d, ϕ_{ra}) pair and the Earth surface $d\Omega_E$, in order to find the effective area of the detector. The resulting plots for the on-shell and off-shell scenarios are demonstrated in the upper-left panel and the lower-left panel of FIG. 10, respectively. We then convolve the results with the χ_1 flux expected from the decay of the heavy dark-matter particle ϕ [see also Eq. (3.4)] and total exposure time of the three flights of ANITA, in order to calculate the differential number of events per emergence angle, i.e., Eq. (4.4). The associated plots for the on-shell and off-shell scenarios appear in the upper-right panel and the lower-right panel of FIG. 10, correspondingly. For reference purpose, we mark the θ_{em} values associated with the two ANITA events by black dashed vertical lines.

In both scenarios we adapt the lifetimes of the decaying particles such that the total expected number of events is of $\mathcal{O}(1)$, given the exposure time $t_{\text{exp}} = 85.5$ days. As can be seen in both the on-shell and off-shell cases, varying

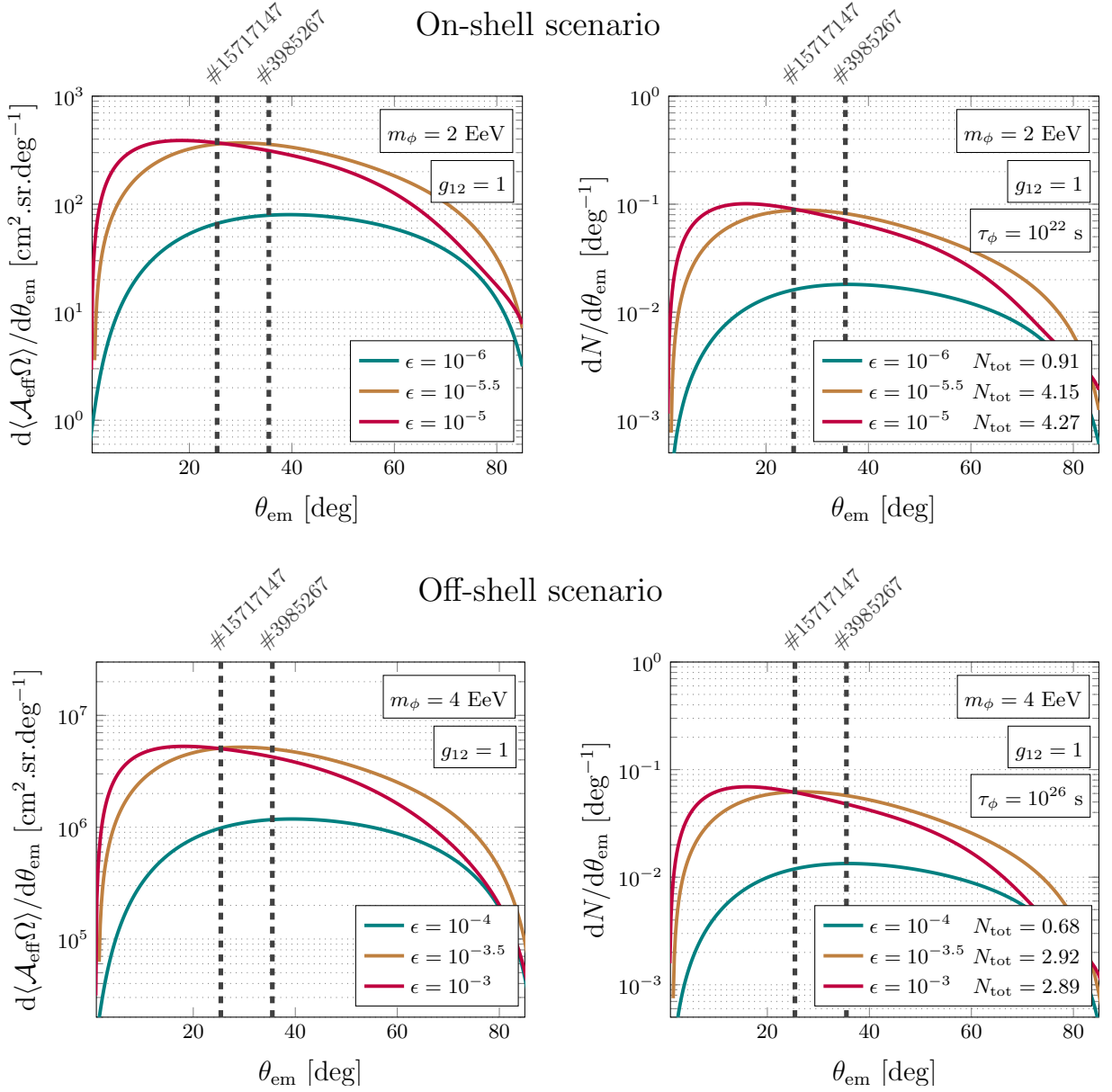


FIG. 10. Total effective area (left panels) and differential number of events (right panels) as a function of the emergence angle θ_{em} anticipated for ANITA-85.5 days, in the cases of “on-shell” scenario (upper panels) and “off-shell” scenario (lower panels). Parameter choices appear in the respective legends.

the value of the kinetic mixing parameter clearly exhibits the transition from the opaque case (large ϵ) to the transparent case (small ϵ). Furthermore, we observe that the maximum value of the angular distribution changes according to what was described in Sec. II. As expected previously, the intermediate case (or translucent case) shows a maximum at emergence angles of $\mathcal{O}(25^\circ - 35^\circ)$, which is the range in which the two anomalous events observed by ANITA are lying.

Finally, we make a brief comment on the relic abundance of χ_1 . Since our benchmark dark-sector model assumes that χ_1 is a negligible relic component, it is crucial to check whether or not our parameter choices indeed

advocate the assumption. We have explicitly calculated the χ_1 relic density for all sets of parameter choices, employing **MicrOMEGAs** [54]. The numerical outcomes suggest that $m_1 \gtrsim 0.45$ GeV in the on-shell scenario and $m_1 \gtrsim 1.9$ GeV in the off-shell scenario be good enough to have negligible ($\lesssim 0.1\%$) abundance for our coupling choices, in addition to the resonance regime satisfying $m_X \simeq 2m_1$.

VI. CONCLUSIONS AND OUTLOOK

The upward-moving anomalous events reported recently by the ANITA Collaboration [1, 2] have brought increasing attention in the particle physics community, as it seems disfavored to explain them under the SM framework, e.g., tau-neutrino-induced processes. Therefore, the phenomenon has been considered as a hint to new physics beyond the SM, stimulating a growing number of phenomenological studies in the context of new physics scenarios [3, 9–17]. In this paper, we conducted a dedicated study on interpreting the ANITA anomaly with scenarios of inelastic boosted dark matter [47].

The proposed model in this paper includes an EeV-range super-heavy (scalar) dark matter ϕ which predominantly decays to a pair of MeV-range (fermionic) dark matter particles χ_1 in the galactic halo in the present universe. Due to the large mass difference between the two dark-matter states, the lighter dark-matter particles χ_1 produced by the decay of the super-heavy candidate ϕ are highly boosted and reach the Earth. An incident χ_1 may therefore upscatter to a heavier, unstable dark-sector state χ_2 via an exchange of dark gauge boson X . χ_2 then decays to χ_1 and hadronic final states through on-shell (off-shell) intermediary X , while X (χ_2) often becomes considerably long-lived. Such a long-lived particle may escape from the Earth, carrying an EeV-scale energy. Once it decays in the atmosphere at a proper altitude, there arises an EAS which can be detected by ANITA.

We then conducted a parameter survey according to our analysis strategy elaborated in Sec. IV. We examined opaque, translucent, and transparent cases (see Sec. II for their definitions) with different parameter choices, and found that the translucent case can accommodate the ANITA events best in the sense that the expected number of signal events is maximized at an emergence angle in-between 25° and 35° . The selected parameter values are consistent with existing constraints. More importantly, the dark-matter relic abundance associated with our parameter choices supports the benchmark dark-sector model assumption that ϕ and χ_1 are the dominant and negligible relic components, respectively. Therefore, the anomalous events observed by the ANITA Collaboration would be considered as a sign of the inelastic boosted dark matter scenario adopted in this study.

We would like to emphasize that in our scenario, the very feeble interaction of the particles propagating through the Earth with nuclei renders detectors such as

the Auger observatory or IceCube far less competitive than ANITA in terms of signal detection, given their small fiducial volume as compared to the volume of the South Pole atmosphere that ANITA utilizes to observe EAS. Indeed, as opposed to scenarios which require to produce boosted tau leptons inside the Earth crust in order to produce EAS in the atmosphere, our scenario simply requires that boosted X or χ_2 particles reach the Earth surface before decaying, hence very unlikely to leave any significant traces in Earth-based detector.

As a final remark, we point out that although our approach is predicated upon a non-minimal boosted dark matter model containing a dark-sector unstable state (χ_2 in this study), scenarios similar to our “on-shell” scenario are available in the minimal boosted dark matter model, by allowing for the following term in the Lagrangian:

$$\mathcal{L}_{\text{int}} \supset g_{11} \bar{\chi}_1 \gamma^\mu \chi_1 X_\mu, \quad (6.1)$$

where g_{11} is the coupling constant governing a χ_1 -flavor-conserving interaction. The existence of this operator, in turn, allows for the process

$$\chi_1 + N \rightarrow \chi_1 + X + \text{anything}, \quad (6.2)$$

by radiating a dark gauge boson X off initial-/final-state χ_1 (called “dark-strahlung”) [55]. This scenario is plausible and the event rate would be sizable especially for smaller m_X and larger g_{11} , compared to those of the current reference parameter sets. It is certainly interesting to distinguish the two possibilities which requires a dedicated study. We leave the exploration of this direction for a future work.

ACKNOWLEDGMENTS

We would like to thank Kim Berghaus, Bhupal Dev, Ian Lewis, Yann Mambrini, Mathias Pierre, and Yicong Sui for useful discussions. The work of L.H. and D.K. is supported by the Department of Energy under Grant DE-FG02-13ER41976 (de-sc0009913). The work of J.-C.P. is supported by the National Research Foundation of Korea (NRF-2019R1C1C1005073 and NRF-2018R1A4A1025334). The work of S.S. is supported by the National Research Foundation of Korea (NRF-2017R1D1A1B03032076 and in partial by NRF-2018R1A4A1025334). A part of this work was discussed in the workshop “Dark Matter as a Portal to New Physics” at Asia Pacific Center for Theoretical Physics in Jan 14th - 18th, 2019.

-
- [1] P. W. Gorham *et al.* (ANITA), Phys. Rev. Lett. **117**, 071101 (2016), arXiv:1603.05218 [astro-ph.HE].
 [2] P. W. Gorham *et al.* (ANITA), Phys. Rev. Lett. **121**, 161102 (2018), arXiv:1803.05088 [astro-ph.HE].

- [3] D. B. Fox, S. Sigurdsson, S. Shandera, P. Mészáros, K. Murase, M. Mostafá, and S. Coutu, Submitted to: Phys. Rev. D (2018), arXiv:1809.09615 [astro-ph.HE].

- [4] A. Romero-Wolf *et al.*, Phys. Rev. **D99**, 063011 (2019), arXiv:1811.07261 [astro-ph.HE].
- [5] A. Aab *et al.* (Pierre Auger), Phys. Rev. **D91**, 092008 (2015), arXiv:1504.05397 [astro-ph.HE].
- [6] M. G. Aartsen *et al.* (IceCube), Phys. Rev. Lett. **117**, 241101 (2016), [Erratum: Phys. Rev. Lett. **119**, no. 25, 259902 (2017)], arXiv:1607.05886 [astro-ph.HE].
- [7] K. D. de Vries and S. Prohira, (2019), arXiv:1903.08750 [astro-ph.HE].
- [8] I. M. Shoemaker, A. Kusenko, P. K. Munneke, A. Romero-Wolf, D. M. Schroeder, and M. J. Siegart, (2019), arXiv:1905.02846 [astro-ph.HE].
- [9] J. F. Cherry and I. M. Shoemaker, Phys. Rev. **D99**, 063016 (2019), arXiv:1802.01611 [hep-ph].
- [10] G.-y. Huang, Phys. Rev. **D98**, 043019 (2018), arXiv:1804.05362 [hep-ph].
- [11] B. Chauhan and S. Mohanty, (2018), arXiv:1812.00919 [hep-ph].
- [12] L. A. Anchordoqui, V. Barger, J. G. Learned, D. Marfatia, and T. J. Weiler, LHEP **1**, 13 (2018), arXiv:1803.11554 [hep-ph].
- [13] J. H. Collins, P. S. Bhupal Dev, and Y. Sui, Phys. Rev. **D99**, 043009 (2019), arXiv:1810.08479 [hep-ph].
- [14] L. A. Anchordoqui and I. Antoniadis, Phys. Lett. **B790**, 578 (2019), arXiv:1812.01520 [hep-ph].
- [15] L. Heurtier, Y. Mambrini, and M. Pierre, (2019), arXiv:1902.04584 [hep-ph].
- [16] D. Hooper, S. Wegsman, C. Deaconu, and A. Vieregge, (2019), arXiv:1904.12865 [astro-ph.HE].
- [17] J. M. Cline, C. Gross, and W. Xue, (2019), arXiv:1904.13396 [hep-ph].
- [18] I. Esteban, J. Lopez-Pavon, I. Martinez-Soler, and J. Salvado, (2019), arXiv:1905.10372 [hep-ph].
- [19] A. Bhattacharya, R. Gandhi, and A. Gupta, JCAP **1503**, 027 (2015), arXiv:1407.3280 [hep-ph].
- [20] J. Kopp, J. Liu, and X.-P. Wang, JHEP **04**, 105 (2015), arXiv:1503.02669 [hep-ph].
- [21] A. M. Dziewonski and D. L. Anderson, Physics of the earth and planetary interiors **25**, 297 (1981).
- [22] L. Heurtier, D. Kim, S. C. Park, J.-C. Park, and S. Shin, (in progress).
- [23] D. J. H. Chung, E. W. Kolb, and A. Riotto, *Neutrino telescopes. Proceedings, 8th International Workshop, Venice, Italy, February 23-26, 1999. Vol. 1, 2*, Phys. Rev. **D59**, 023501 (1999), arXiv:hep-ph/9802238 [hep-ph].
- [24] D. J. H. Chung, E. W. Kolb, and A. Riotto, Phys. Rev. Lett. **81**, 4048 (1998), arXiv:hep-ph/9805473 [hep-ph].
- [25] J. F. Navarro, C. S. Frenk, and S. D. M. White, Astrophys. J. **462**, 563 (1996), arXiv:astro-ph/9508025 [astro-ph].
- [26] J. F. Navarro, C. S. Frenk, and S. D. M. White, Astrophys. J. **490**, 493 (1997), arXiv:astro-ph/9611107 [astro-ph].
- [27] D. Kim, P. A. N. Machado, J.-C. Park, and S. Shin, (in progress).
- [28] A. D. Martin, W. J. Stirling, R. S. Thorne, and G. Watt, Eur. Phys. J. **C63**, 189 (2009), arXiv:0901.0002 [hep-ph].
- [29] S. Aid *et al.* (H1), Z. Phys. **C69**, 27 (1995), arXiv:hep-ex/9509001 [hep-ex].
- [30] H. Abramowicz *et al.* (ZEUS), Phys. Lett. **B697**, 184 (2011), arXiv:1011.1652 [hep-ex].
- [31] G. F. Giudice, D. Kim, J.-C. Park, and S. Shin, Phys. Lett. **B780**, 543 (2018), arXiv:1712.07126 [hep-ph].
- [32] D. P. Finkbeiner and N. Weiner, Phys. Rev. **D76**, 083519 (2007), arXiv:astro-ph/0702587 [astro-ph].
- [33] N. Arkani-Hamed, D. P. Finkbeiner, T. R. Slatyer, and N. Weiner, Phys. Rev. **D79**, 015014 (2009), arXiv:0810.0713 [hep-ph].
- [34] M. Pospelov and A. Ritz, Phys. Lett. **B671**, 391 (2009), arXiv:0810.1502 [hep-ph].
- [35] D. P. Finkbeiner, T. R. Slatyer, N. Weiner, and I. Yavin, JCAP **0909**, 037 (2009), arXiv:0903.1037 [hep-ph].
- [36] D. Kim, J.-C. Park, and S. Shin, JHEP **04**, 093 (2018), arXiv:1702.02944 [hep-ph].
- [37] R. Essig, Phys. Rev. **D78**, 015004 (2008), arXiv:0710.1668 [hep-ph].
- [38] N. Arkani-Hamed and N. Weiner, JHEP **12**, 104 (2008), arXiv:0810.0714 [hep-ph].
- [39] Y. Bai and T. M. P. Tait, Phys. Lett. **B710**, 335 (2012), arXiv:1109.4144 [hep-ph].
- [40] N. F. Bell, Y. Cai, and A. D. Medina, Phys. Rev. **D89**, 115001 (2014), arXiv:1311.6169 [hep-ph].
- [41] E. Izaguirre, G. Krnjaic, P. Schuster, and N. Toro, Phys. Rev. **D90**, 014052 (2014), arXiv:1403.6826 [hep-ph].
- [42] E. Izaguirre, Y. Kahn, G. Krnjaic, and M. Moschella, Phys. Rev. **D96**, 055007 (2017), arXiv:1703.06881 [hep-ph].
- [43] A. Berlin, S. Gori, P. Schuster, and N. Toro, Phys. Rev. **D98**, 035011 (2018), arXiv:1804.00661 [hep-ph].
- [44] A. Berlin and F. Kling, Phys. Rev. **D99**, 015021 (2019), arXiv:1810.01879 [hep-ph].
- [45] P. Coloma, P. A. N. Machado, I. Martinez-Soler, and I. M. Shoemaker, Phys. Rev. Lett. **119**, 201804 (2017), arXiv:1707.08573 [hep-ph].
- [46] P. Coloma, (2019), arXiv:1906.02106 [hep-ph].
- [47] D. Kim, J.-C. Park, and S. Shin, Phys. Rev. Lett. **119**, 161801 (2017), arXiv:1612.06867 [hep-ph].
- [48] A. Chatterjee, A. De Roeck, D. Kim, Z. G. Moghaddam, J.-C. Park, S. Shin, L. H. Whitehead, and J. Yu, Phys. Rev. **D98**, 075027 (2018), arXiv:1803.03264 [hep-ph].
- [49] M. Pospelov, N. Weiner, and I. Yavin, Phys. Rev. **D89**, 055008 (2014), arXiv:1312.1363 [hep-ph].
- [50] Y. Grossman, R. Harnik, O. Telem, and Y. Zhang, (2017), arXiv:1712.00455 [hep-ph].
- [51] J. Eby, P. J. Fox, R. Harnik, and G. D. Kribs, (2019), arXiv:1904.09994 [hep-ph].
- [52] J. Alvarez-Muñiz, W. R. Carvalho, A. L. Cummings, K. Payet, A. Romero-Wolf, H. Schoorlemmer, and E. Zas, Phys. Rev. **D97**, 023021 (2018), [erratum: Phys. Rev. **D99**, no. 6, 069902 (2019)], arXiv:1707.00334 [astro-ph.HE].
- [53] T. Sjostrand, S. Ask, J. R. Christiansen, R. Corke, N. Desai, P. Ilten, S. Mrenna, S. Prestel, C. O. Rasmussen, and P. Z. Skands, Comput. Phys. Commun. **191**, 159 (2015), arXiv:1410.3012 [hep-ph].
- [54] G. Bélanger, F. Boudjema, A. Goudelis, A. Pukhov, and B. Zaldivar, Comput. Phys. Commun. **231**, 173 (2018), arXiv:1801.03509 [hep-ph].
- [55] D. Kim, J.-C. Park, and S. Shin, (2019), arXiv:1903.05087 [hep-ph].